IEEE Access
Multidisciplinary | Rapid Review | Open Access Journal

Received May 30, 2019, accepted July 12, 2019, date of publication July 22, 2019, date of current version August 6, 2019.

*Digital Object Identifier 10.1109/ACCESS.2019.2929830*

# A Novel Multi-Criteria Preamble Detection Algorithm for ADS-B Signals

**PENG REN[1], JIANXIN WANG[1], HAIWEI SONG[2], PEIXIN ZHANG[1], AND TIAN BAN[1]**
[1]School of Electronic and Optical Engineering, Nanjing University of Science and Technology, Nanjing 210094, China
[2]Nanjing Electronic Equipment Institute, Nanjing 210007, China

Corresponding author: Jianxin Wang (wangjxin@njust.edu.cn)

**ABSTRACT** Satellite-based automatic dependent surveillance broadcast (ADS-B) is of great importance in the next generation air traffic management system. However, there are two major challenges: interference and low signal to noise ratio (SNR). The interference can be mitigated by various separation algorithms. In this paper, we are committed to improving the detection performance for the ADS-B signals with downlink format field equal to 17 at low SNRs. At the moment, commercial receivers work well with sufficient SNRs but may not function properly in the case of the low SNRs. To this end, based on the characteristics of the ADS-B signal frame format, we propose a novel multi-criteria preamble detection algorithm. The proposed algorithm is a constant false alarm rate (CFAR) detection algorithm, and the determination of threshold is independent of noise power. We make a detailed theoretical analysis of each criterion, and develop the analytic expression of the detection probability. All the theoretical results are validated by the Monte Carlo simulations. The simulation shows that the proposed algorithm has an excellent probability of detection when the SNR is low, which is suitable for the satellite-based ADS-B application.

**INDEX TERMS** ADS-B, low SNR, multi-criteria, preamble detection, theoretical analysis.

## I. INTRODUCTION

With the rapid growth of civil aviation transportation business, the air-traffic flow is supposed to provide more feasible utilization of airspace levels and capacities so as to meet the demands of the next generation air traffic management (ATM) system [1]. Apart from the secondary surveillance radar, automatic dependent surveillance broadcast (ADS-B) is another efficient and superior technology used for air traffic control. An aircraft retrieves its own position and velocity via satellite navigation, and broadcasts them to the ground stations and other aircraft nearby to improve situational awareness [2]. The advent of ADS-B may bring several benefits in safety, capacity and efficiency [3]–[6]. First of all, the flight separation could be reduced dramatically. ADS-B is much more cost-effective compared with the radar infrastructure. Besides, the reduction in fuel consumption makes ADS-B friendly to environment. Hence, ADS-B is being rolled out widely all over the world. In 2010, a final rule was published by the Federal Aviation Administration to mandate that all aircraft should be equipped with ADS-B by the year 2020 [7], [8]. In Europe, ADS-B has been implemented rapidly as a vital component of the Single European Sky ATM Research (SESAR) [9], [10]. Moreover, large expanses of Australia and Canada have been deployed with plenty of ADS-B receiving stations in order to achieve full continental surveillance coverage [11]. However, in some areas like ocean where ADS-B ground stations are inapplicable, satellite-based ADS-B application shall be a promising solution to enhance the ATM.

The satellite-based ADS-B application has attracted a great deal of interest at the moment. Reference [12] introduced the world's first in-orbit demonstration of a space based ADS-B, as well as the GATOSS mission in [13] and Iridium NEXT satellite in [14]. Nevertheless, there are two major challenges for the reception of satellite-based ADS-B signals: interference and low signal to noise ratio (SNR). The interference arises from that ADS-B signals share the same 1090 MHz frequency with Mode A/C and Mode S replies [15]. Sectorized antennas might be a useful method to mitigate the interference because it exploits a spatial diversity through the use of multiple directive antenna beams [16].

The associate editor coordinating the review of this manuscript and approving it for publication was Liangtian Wan.

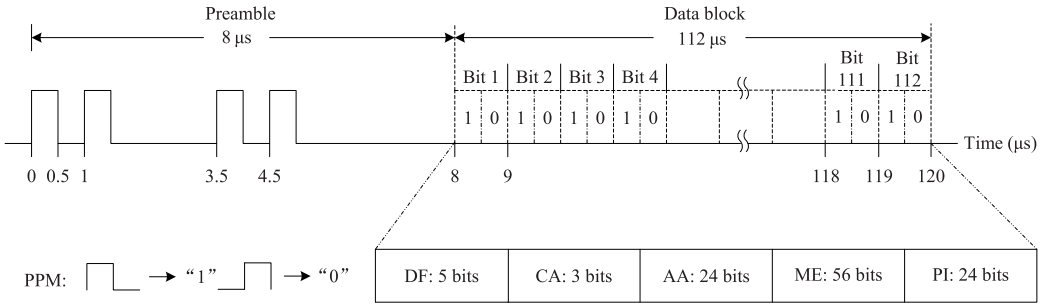


**FIGURE 1.** Frame format of ADS-B signals.

Also, there are various separation algorithms that are aimed to separate the overlapping signals, such as EPA, MDA, MS-ZCMA, PASA, etc [17]–[22]. After the separation, it is still necessary to detect the weak ADS-B signals. In this paper, we are committed to solving the problem of how to improve the detection performance in the case of low SNRs. The widely used enhanced preamble detection algorithm recommended in [23] has an excellent performance with sufficient SNRs. When it is applied to the satellite, the detection performance would be deteriorated sharply due to the insufficient receiving signal power. As shown in [12], the majority of received Mode S signals from space have a signal power of maximal $-89$ dBm and $-103$ dBm minimal. In addition, by analyzing the received ADS-B messages collected in OpenSky, a sensor network consisting of 11 sensors located in central Europe, a conclusion can be drawn that the SNRs of correctly decoded messages range from 2.71 dB to 33.13 dB, with the 0.5 and 99.5 percent quantiles at 7.64 dB and 21.79 dB, respectively [11]. Thus, low SNR is a non-negligible factor that restricts the reception of satellite-based ADS-B signals.

To this end, upon investigating the characteristics of signal format, we propose a novel multi-criteria preamble detection algorithm for ADS-B signals. As stipulated in [23], an ADS-B message contains five different fields in the data block, i.e., downlink format field (DF), capability field (or control field, application field), address field, message, and parity/identity field, which is shown in Fig. 1. The DF occupies the first five symbols of the data block, and the value of 17 (i.e., DF $=$ 17, binary 10001) is assigned to all ADS-B message transmissions from Mode S transponder-based devices [24], which are equipped by most aircraft. Hence, the proposed detection algorithm is designed for ADS-B signals with DF set to 17. There are four criteria in the proposed algorithm, i.e., constant false alarm rate (CFAR) detection, deterministic symbol match, consistent power test and null symbol validation. The first criterion is implemented by comparing the test statistic with a predetermined threshold. The threshold depends on the desired probability of false alarm and is independent of noise power. The subsequent three criteria aim to further identify the ADS-B preamble and suppress the false alarm. When all the criteria are satisfied, an ADS-B preamble is declared to be detected. The proposed algorithm is of the CFAR property and is robust against noise fluctuation. We also conduct a detailed theoretical analysis of each criterion, and develop the analytic expression for the detection probability. Monte Carlo simulations are carried out to validate the theoretical results. By comparing the proposed algorithm with that in [23], we find that the proposed algorithm has an excellent detection performance in the case of low SNRs, and is suitable for satellite-based ADS-B application.

The remainder of this paper is organized as follows. The signal model is established in section II. In section III – VI, the four criteria are elaborated, including the theoretical analysis. The simulations and results are presented in section VII, followed by the conclusion in section VIII.

## II. SIGNAL MODEL

An ADS-B 1090 MHz Mode S extended squitter (1090ES) message consists of a preamble of 8 $\mu$s and a data block of 112 $\mu$s. In the data block, there are 112 binary symbols, which can be expressed as $\mathbf{s} = [s[1], s[2], \ldots, s[112]]$. The symbol period is 1 $\mu$s and each symbol is made up by two 0.5 $\mu$s chips. As shown in [25], each $s[k]$ $(k = 1, 2, \ldots, 112)$ is Manchester encoded, using the mapping relation of which we can obtain the corresponding bit sequence of date block, i.e., $\mathbf{b} = [b[1], b[2], \ldots, b[224]]$ where

$$\begin{cases} b[2k-1]=1 \quad b[2k]=0 \text{ if } s[k]=1 \\ b[2k-1]=0 \quad b[2k]=1 \text{ if } s[k]=0 \end{cases}, \quad k=1, 2, \ldots, 112.$$

For all the ADS-B 1090ES messages, the preamble bit sequence is identical and can be written as $\mathbf{p} = [1, 0, 1, 0, 0, 0, 0, 1, 0, 1, 0, 0, 0, 0, 0, 0]$. Therefore, the bit sequence of a whole ADS-B message can be expressed as the stack of the preamble bit sequence and the data block bit sequence, i.e., $\mathbf{d} = [\mathbf{p}, \mathbf{b}]$. There are totally 240 elements in the bit sequence $\mathbf{d}$.

The block diagram of the proposed multi-criteria preamble detection algorithm is shown in Fig. 2.

Assuming that the ADS-B message is present, the received baseband in-phase and quadrature (I/Q) components have the

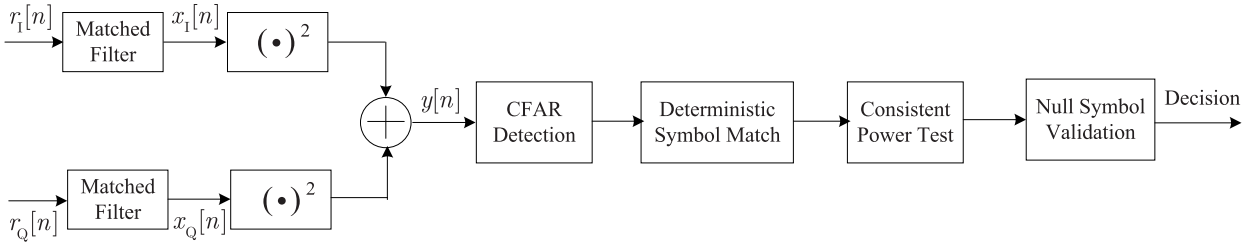


**FIGURE 2.** Block diagram of multi-criteria preamble detection algorithm.

form

$$r_I[n] = A\sum_{i=1}^{240} d[i]u[n-iL]\cos(\varpi_d n+\varphi_0) + w_I[n]$$
$$r_Q[n] = A\sum_{i=1}^{240} d[i]u[n-iL]\sin(\varpi_d n+\varphi_0) + w_Q[n], \quad (1)$$

where $A$ is the amplitude of the received signal, $d[i]$ is the $i$th element in the bit sequence $\mathbf{d}$. Here we assume that the sampling rate of $r_I[n]$ and $r_Q[n]$ denoted by $f_s$ is equal to 18 MHz. $u[n]$ is the sampled version of a rectangular pulse with width $T_b = 0.5\ \mu$s, $L = f_s T_b = 9$ is the number of samples per rectangular pulse. $\varpi_d = 2\pi\Delta f/f_s$ is the normalized residual digital angular frequency in which $\Delta f$ is the frequency offset. $\varphi_0$ is the residual phase which is unknown but fixed for a single ADS-B message and is uniformly distributed in the interval $[0, 2\pi)$. $w_I[n]$ and $w_Q[n]$ are white Gaussian noise which is assumed to be a zero-mean stationary and uncorrelated discrete random process, i.e., $E[w_I[n]] = E[w_Q[n]] = 0$ and $Var[w_I[n]] = Var[w_Q[n]] = \sigma^2$, where $\sigma^2$ is the noise power.

For simplicity of analysis, it is supposed that there is no frequency offset in the received signal, that is $\varpi_d = 0$. Equation (1) reduces to

$$r_I[n] = A\sum_{i=1}^{240} d[i]u[n-iL]\cos\varphi_0 + w_I[n]$$
$$r_Q[n] = A\sum_{i=1}^{240} d[i]u[n-iL]\sin\varphi_0 + w_Q[n]. \quad (2)$$

As described in Fig. 2, the received I/Q components $r_I[n]$ and $r_Q[n]$ are firstly presented to the matched filters with impulse response $g[n] = 1/L$ for $0 \le n \le L-1$. Hence, the output sequences $x_I[n]$ and $x_Q[n]$ of the matched filters can be expressed in the form of convolution of input sequences and impulse response, i.e.,

$$x_I[n] = r_I[n]\otimes g[n] = A\cos(\varphi_0)\sum_{i=1}^{240} d[i]v[n-iL] + w'_I[n]$$
$$x_Q[n] = r_Q[n]\otimes g[n] = A\sin(\varphi_0)\sum_{i=1}^{240} d[i]v[n-iL] + w'_Q[n], \quad (3)$$

where $\otimes$ is the convolution operator, $v[n] = u[n]\otimes g[n]$, $w'_I[n] = w_I[n]\otimes g[n]$ is the output noise sequence of the matched filter excited by the white Gaussian noise $w_I[n]$, as well as $w'_Q[n]$. Let $y[n]$ denote the squared amplitude sequence of $x_I[n]$ and $x_Q[n]$. According to (3), we can obtain the expression of $y[n]$ as follows

$$y[n] = x_I^2[n] + x_Q^2[n] = \left(A\sum_{i=1}^{240} d[i]v[n-iL]\right)^2 + z[n], \quad (4)$$

where

$$z[n] = 2A\sum_{i=1}^{240} d[i]v[n-iL](w'_I[n]\cos\varphi_0 + w'_Q[n]\sin\varphi_0) + w_I'^2[n] + w_Q'^2[n]$$

is a term in relation to noise. All further processing would be applied to the squared amplitude sequence $y[n]$.

## III. CFAR DETECTION

### A. DESCRIPTION

For every ADS-B message with DF = 17, the first 26 elements in $\mathbf{d}$ are fixed and can be defined as the characteristic word represented as

$$\mathbf{e} = [1,0,1,0,0,0,0,1,0,1,0,0,0,0,0,0,0,1,0,0,1,0,1,0,1,1,0]. \quad (5)$$

Hence, we have the target to detect the occurrence of such a sequence in the received signal for preamble detection in principle.

In order to improve the correlation properties, the 8 $\mu$s preamble and 5 $\mu$s DF field are used jointly for correlation in the proposed algorithm. Matched filters have already been employed and the squared amplitude sequence $y[n]$ is no longer composed of rectangular pulses. Hence, we select the reference sequence $h[n]$ of length $26L$ (corresponding to 13 $\mu$s in the analog domain), which comprises only 9 nonzero values at fixed positions. The expression of the reference sequence is given by

$$h[n] = \sum_{j=1}^{26} e[j]\delta[n-jL] \quad \text{for } 1 \le n \le 26L, \quad (6)$$

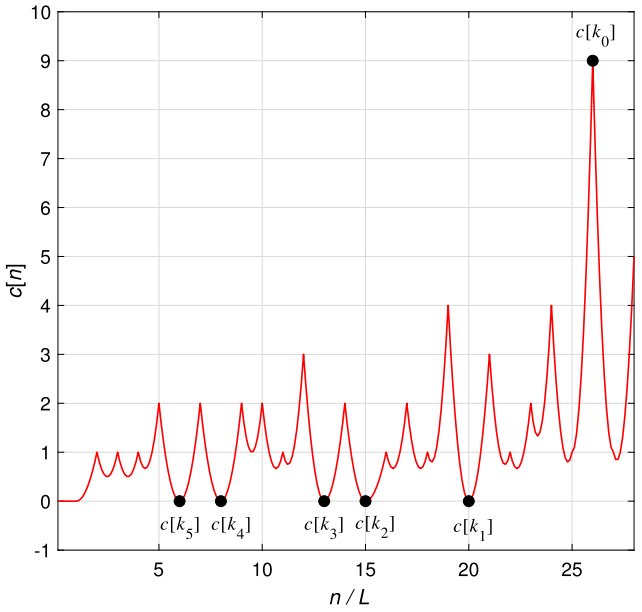


**FIGURE 3.** Waveform of correlation values for $A = 1$.

where $e[j]$ is the $j$th element in the characteristic word $\mathbf{e}$ of (5) and $\delta[n]$ is the unit sample sequence.

Then the correlation properties are examined. In noise-free situations, the squared amplitude sequence has the form $y[n] = (A\sum_{i=1}^{240} d[i]v[n-iL])^2$. We take a special case with $n = kL$ $(k = 1, 2, \ldots, 240)$ into consideration, yielding $y[kL] = A^2 d[k]$. The noise-free squared amplitude sequence $y[n]$ is presented to the correlator with reference sequence $h[n]$, the output of which can be written as

$$c[n] = y[n] \otimes h[26L - n] = \sum_{j=1}^{26} e[j]y[n - 26L + jL]. \quad (7)$$

Next, we investigate the values of $c[n]$ at specific instants. The instants under consideration are set to be $n = 26L$, $20L$, $15L$, $13L$, $8L$, $6L$, which are expressed by $k_0$, $k_1$, $k_2$, $k_3$, $k_4$, and $k_5$ respectively. For $n = k_0$, the value of $c[k_0]$ can be calculated as follows:

$$c[k_0] = A^2 \sum_{j=1}^{26} e[j]d[j] = 9A^2. \quad (8)$$

Similarly, we have the following equations for $n = k_1$, $k_2$, $k_3$, $k_4$, and $k_5$

$$c[k_1] = c[k_2] = c[k_3] = c[k_4] = c[k_5] = 0. \quad (9)$$

According to (8) and (9), it is clear that the maximum peak value can be achieved for $n = 26L$ when the received preamble and the reference sequence are aligned exactly. Moreover, for $n = 20L$, $15L$, $13L$, $8L$, and $6L$, the correlation value $c[n]$ reaches the valley values that are nominally equal to zero. An example for the waveform of correlation value with $A = 1$ is shown in Fig. 3.

The detection algorithm in this paper defines the test statistic as the ratio of the peak value to the average of the five valley values, i.e.,

$$T = \frac{c[k_0]}{\frac{1}{5}\sum_{i=1}^{5} c[k_i]}. \quad (10)$$

When $T$ is larger than or equal to a predetermined threshold $\lambda_c$, the second criterion deterministic symbol match is activated. The detection threshold depends on the false alarm probability of the CFAR detection.

### B. ANALYSIS OF CFAR DETECTION

First of all, the hypothesis testing model can be described as follows:

$$\begin{aligned} H_1 &: y[n] = \left(A\sum_{i=1}^{240} d[i]v[n-iL]\right)^2 + z[n] \\ H_0 &: y[n] = w_{\mathrm{I}}'^2[n] + w_{\mathrm{Q}}'^2[n]. \end{aligned} \quad (11)$$

In order to derive the success probability of the CFAR detection, it is necessary to analyze the distribution of squared amplitude sequence under the hypothesis $H_1$ briefly. Herein, we concentrate on the instant $n = iL$ $(i = 1, 2, \ldots, 240)$ only. Thus, the expressions of $x_{\mathrm{I}}[n]$ and $x_{\mathrm{Q}}[n]$ at instant $n = iL$ can be rewritten as

$$\begin{aligned} x_{\mathrm{I}}[iL] &= A\cos(\varphi_0)d[i] + \frac{1}{9}\sum_{j=iL-8}^{iL} w_{\mathrm{I}}[j] \\ x_{\mathrm{Q}}[iL] &= A\sin(\varphi_0)d[i] + \frac{1}{9}\sum_{j=iL-8}^{iL} w_{\mathrm{Q}}[j]. \end{aligned} \quad (12)$$

The $i$th element $d[i]$ in the bit sequence $\mathbf{d}$ is a binary variable, and $d[i] \in \{0,\ 1\}$.

If $d[i] = 1$, both $x_{\mathrm{I}}[iL]$ and $x_{\mathrm{Q}}[iL]$ are random Gaussian variables with variance $\sigma^2/9$ and means equal to $A\cos\varphi_0$ and $A\sin\varphi_0$ respectively. The sum of the square of two nonzero mean independent Gaussian random variables leads to a non-central chi-squared random variable with two degrees of freedom [26]. The squared amplitude sequence $y[iL] = x_{\mathrm{I}}^2[iL] + x_{\mathrm{Q}}^2[iL]$ for $d[i] = 1$ is subject to the non-central chi-squared distribution with a non-centrality parameter equal to $A^2$.

If $d[i] = 0$, it is obvious that $x_{\mathrm{I}}[iL] \sim N(0,\ \sigma^2/9)$ and $x_{\mathrm{Q}}[iL] \sim N(0,\ \sigma^2/9)$. The sum of the square of two zero-mean independent Gaussian random variables leads to a central chi-squared random variable with two degrees of freedom (aka exponentially distribution with parameter $9/2\sigma^2$ [27]). Hence, we have $y[iL] \sim \chi_2^2$ for $d[i] = 0$.

Due to the properties of the preamble and pulse position modulation (PPM) scheme, only 9 elements in the characteristic word $\mathbf{e}$ of (5) are nonzero, the index vector of which can be constructed as follows:

$$\boldsymbol{\alpha} = [1, 3, 8, 10, 17, 20, 22, 24, 25]. \quad (13)$$

According to (7), the numerator of the test statistic $T$ can be represented as

$$c[k_0] = \sum_{j=1}^{26} e[j]y[jL] = \sum_{i=1}^{9} \gamma[i], \tag{14}$$

in which $\gamma[i] = y[\alpha[i]L]$ $(i = 1, 2, \ldots, 9)$ and $\alpha[i]$ being the $i$th element of the index vector $\boldsymbol{\alpha}$. As analyzed above, $\gamma[i]$ $(i = 1, 2, \ldots, 9)$ is subject to the non-central chi-squared distribution with two degrees of freedom and a non-centrality parameter equal to $A^2$.

Similarly, for the denominator of the test statistic $T$, we have

$$\begin{aligned}
c[k_1] &= \sum_{i=1}^{9} y[(\alpha[i] - 6)L] \\
c[k_2] &= \sum_{i=1}^{9} y[(\alpha[i] - 11)L] \\
c[k_3] &= \sum_{i=1}^{9} y[(\alpha[i] - 13)L] \\
c[k_4] &= \sum_{i=1}^{9} y[(\alpha[i] - 18)L] \\
c[k_5] &= \sum_{i=1}^{9} y[(\alpha[i] - 20)L].
\end{aligned} \tag{15}$$

It is apparent that the denominator of $T$ is the sum of 45 random variables, some of which, however, are duplicated. There are totally 23 different variables in the denominator, nine of which added once, nine of which added twice, two of which added three times and the rest added four times. Thus, the denominator can be rewritten as

$$\begin{aligned}
\frac{1}{5}\sum_{i=1}^{5} c[k_i] = \frac{1}{5}\sum_{i=1}^{9} \eta[i] + \frac{2}{5}\sum_{i=10}^{18} \eta[i] \\
+ \frac{3}{5}\sum_{i=19}^{20} \eta[i] + \frac{4}{5}\sum_{i=21}^{23} \eta[i]
\end{aligned} \tag{16}$$

where $\eta[i]$ is the $i$th element in $\boldsymbol{\eta}$ that is given as follows:

$$\begin{aligned}
\boldsymbol{\eta} = [&y[-19L], y[-15L], y[0], y[5L], y[12L], y[13L], y[16], \\
&y[18L], y[19L], y[-17L], y[-12L], y[-8L], y[-5L], \\
&y[-L], y[6L], y[7L], y[9L], y[14L], y[2L], y[11L], \\
&y[-10L], y[-3L], y[4L]].
\end{aligned} \tag{17}$$

Each $\eta[i]$ $(i = 1, 2, \ldots, 23)$ in (16) is a central chi-squared random variable with two degrees of freedom.

Substituting (14) and (16) into (10), and multiplying the numerator and denominator by a factor of $9/\sigma^2$ respectively, we obtain

$$T = \frac{\sum_{i=1}^{9} \gamma[i]\frac{9}{\sigma^2}}{\frac{9}{\sigma^2}\left(\frac{1}{5}\sum_{i=1}^{9}\eta[i] + \frac{2}{5}\sum_{i=10}^{18}\eta[i] + \frac{3}{5}\sum_{i=19}^{20}\eta[i] + \frac{4}{5}\sum_{i=21}^{23}\eta[i]\right)}. \tag{18}$$

For simplicity of expression, let $\widetilde{\gamma}[i] = 9\gamma[i]/\sigma^2$, $i = 1, 2, \ldots, 9$. According to the distribution of $\gamma[i]$, it is obvious that $\widetilde{\gamma}[i]$ is subject to the non-central chi-squared distribution with two degrees of freedom, and the non-centrality parameter of $\widetilde{\gamma}[i]$ is equal to $9A^2/\sigma^2$.

Let $\widetilde{\eta}[i] = 9l_i\eta[i]/5\sigma^2$ in which

$$l_i = \begin{cases} 1 & \text{for } i = 1, 2, \ldots, 9 \\ 2 & \text{for } i = 10, 11, \ldots, 18 \\ 3 & \text{for } i = 19, 20 \\ 4 & \text{for } i = 21, 22, 23. \end{cases} \tag{19}$$

Considering $\eta[i] \sim \chi_2^2$ $(i = 1, 2, \ldots, 23)$, we can see that $\widetilde{\eta}[i]$ $(i = 1, 2, \ldots, 23)$ are also central chi-squared random variables with two degrees of freedom. However, the variances of $\widetilde{\eta}[i]$ are no longer the same. Then $\widetilde{\eta}[i]$ $(i = 1, 2, \ldots, 23)$ can be divided into four sets depending on the variances. To be specific, the variance of the variables in the set $\{\widetilde{\eta}[i],\ i = 1, 2, \ldots, 9\}$ is denoted by $\sigma_1^2$; the variance of the variables in the set $\{\widetilde{\eta}[i],\ i = 10, 11, \ldots, 18\}$ is denoted by $\sigma_2^2$; the variance of the variables in the set $\{\widetilde{\eta}[i],\ i = 19, 20\}$ is denoted by $\sigma_3^2$; and the variance of the variables in the set $\{\widetilde{\eta}[i],\ i = 21, 22, 23\}$ is denoted by $\sigma_4^2$, i.e.,

$$\begin{cases} \sigma_1^2 = 2/5 & \text{for } \widetilde{\eta}[i] \text{ with } i = 1, 2, \ldots, 9 \\ \sigma_2^2 = 4/5 & \text{for } \widetilde{\eta}[i] \text{ with } i = 10, 11, \ldots, 18 \\ \sigma_3^2 = 6/5 & \text{for } \widetilde{\eta}[i] \text{ with } i = 19, 20 \\ \sigma_4^2 = 8/5 & \text{for } \widetilde{\eta}[i] \text{ with } i = 21, 22, 23. \end{cases} \tag{20}$$

The test statistic $T$ of (18) can be written in a more concise form as follows:

$$T = \frac{\sum_{i=1}^{9} \widetilde{\gamma}[i]}{\sum_{i=1}^{23} \widetilde{\eta}[i]} \triangleq \frac{T_{num}}{T_{den}}. \tag{21}$$

From (21), the numerator $T_{num}$ is expressed as the sum of nine independent non-central chi-squared variables with two degrees of freedom. According to the additivity of the non-central chi-squared distribution, $T_{num}$ is a non-central chi-squared random variable with 18 degrees of freedom and a non-centrality parameter equal to $81A^2/\sigma^2$, the probability density function (p.d.f) of which can be expressed as

$$\begin{aligned}
&f_{num}(x\,|H_1) \\
&= \frac{1}{2}\exp\left(-\frac{x + 81A^2/\sigma^2}{2}\right)\left(\frac{x}{81A^2/\sigma 2}\right)^4 I_8\left(\frac{9A}{\sigma}\sqrt{x}\right),
\end{aligned} \tag{22}$$

where $I_8(\cdot)$ is the modified Bessel function of the first kind and order eight.

Then we take the denominator of the test statistic into consideration. The 23 terms in the summation of $T_{den}$ have been divided into four sets, each representing a certain variance value. Let $r_m$ ($m = 1, 2, 3, 4$) denote the number of variables in the $m$th set, and we have $[r_1, r_2, r_3, r_4] = [9, 9, 2, 3]$. Accordingly, $T_{den}$ is subject to the generalized chi-squared distribution [28], of which the p.d.f is given by

$$f_{den}(y\,|H_1) = \prod_{m=1}^{4} \frac{1}{\sigma_m^{2r_m}} \sum_{k=1}^{4} \sum_{l=1}^{r_k} \frac{\Psi_{k,l,r}}{(r_k - l)!}(-y)^{r_k - l} e^{-\frac{y}{\sigma_k^2}} = L_1 \sum_{k=1}^{4} \sum_{l=1}^{r_k} \frac{\Psi_{k,l,r}}{(r_k - l)!}(-y)^{r_k - l} e^{-\frac{y}{\sigma_k^2}}, \tag{23}$$

where $L_1 = \prod_{m=1}^{4} \frac{1}{\sigma_m^{2r_m}}$ is a constant and

$$\Psi_{k,l,r} = (-1)^{r_k - 1} \sum_{i \in \Omega_{k,l}} \prod_{j \neq k} C_{i_j + r_j - 1}^{i_j} \left( \frac{1}{\sigma_j^2} - \frac{1}{\sigma_k^2} \right)^{-(r_j + i_j)} \tag{24}$$

with $[i_1, i_2, i_3, i_4]$ from the set $\Omega_{k,l}$ of all partitions of $l - 1$ (with $i_k = 0$) defined as

$$\Omega_{k,l} = \left\{ [i_1, i_2, i_3, i_4] \in \mathbb{Z}^4; \sum_{j=1}^{4} i_j = l - 1, i_k = 0, i_j \geq 0 \ \forall j \right\}. \tag{25}$$

Note that the notation of the form $C_m^n$ in (24) is the number of $n$-combinations of $m$ and defined as $C_m^n = m!/n!(m - n)!$.

The distributions of the numerator and denominator of the test statistic have already been derived, so the test statistic $T$ has the distribution which can be constructed as the quotient distribution of two independent random variables [29], i.e.,

$$f_T(z\,|H_1) = \int_{-\infty}^{+\infty} |y| f_{num}(yz\,|H_1) f_{den}(y\,|H_1)\mathrm{d}y = \frac{L_1 e^{-\frac{m_1}{2}} z^4}{2m_1^4} \sum_{k=1}^{4} \sum_{l=1}^{r_k} \frac{\Psi_{k,l,r}}{(r_k - l)!}(-1)^{r_k - l} F(k, l), \tag{26}$$

where $m_1 = 81A^2/\sigma^2$ is a parameter proportional to the SNR and

$$F(k, l) = \int_0^{+\infty} y^{r_k - l + 5} \exp\left( -y \left( \frac{z}{2} + \frac{1}{\sigma_k^2} \right) \right) I_8\left( \sqrt{yzm_1} \right) \mathrm{d}y. \tag{27}$$

For a given predetermined threshold $\lambda_c$, the success probability of CFAR detection can be calculated by integrating $f_T(z\,|H_1)$ from $\lambda_c$ to positive infinity, i.e.,

$$P_C = \int_{\lambda_c}^{+\infty} f_T(z\,|H_1)\mathrm{d}y. \tag{28}$$

The value of $P_C$ can be attained by numerical integration. Equation (28) shows that the probability of success $P_C$ is a function of SNR and detection threshold.

### C. DETERMINATION OF THRESHOLD $\lambda_c$

We investigate the false alarm probability of the CFAR detection by which the threshold $\lambda_c$ is determined. Under the null hypothesis $H_0$, the output sequences $x_{\mathrm{I}}[n]$ and $x_{\mathrm{Q}}[n]$ of the matched filters have the form

$$x_{\mathrm{I}}[n] = \frac{1}{9} \sum_{i=n-8}^{n} w_{\mathrm{I}}[i]$$
$$x_{\mathrm{Q}}[n] = \frac{1}{9} \sum_{i=n-8}^{n} w_{\mathrm{Q}}[i], \tag{29}$$

where $w_{\mathrm{I}}[i] \sim N(0, \sigma^2)$ and $w_{\mathrm{Q}}[i] \sim N(0, \sigma^2)$ for $i = n - 8, \ldots, n$. Thus, for a given $n$, $x_{\mathrm{I}}[n]$ is a Gaussian random variable with zero mean and variance $\sigma^2/9$, as well as $x_{\mathrm{Q}}[n]$. So the squared amplitude sequence $y[n] = x_{\mathrm{I}}^2[n] + x_{\mathrm{Q}}^2[n]$ is subject to the central chi-squared distribution with two degrees of freedom.

Then, we consider the numerator of the test statistic under hypothesis $H_0$, which can be written as

$$c[k_0] = \sum_{j=1}^{26} e[j]y[jL] = \sum_{i=1}^{9} \xi[i], \tag{30}$$

where $\xi[i] = y\,[\alpha[i] \cdot L]$ ($i = 1, 2, \ldots, 9$) and $\xi[i]$ are independent identically distributed, i.e., $\xi[i] \sim \chi_2^2$. For the denominator, it can be expressed the same as that of (16) under hypothesis $H_1$. Similarly, via multiplying the numerator and denominator by a factor of $9/\sigma^2$, we can obtain

$$T = \frac{\sum_{i=1}^{9} \xi[i] \frac{9}{\sigma^2}}{\frac{9}{\sigma^2}\left( \frac{1}{5} \sum_{i=1}^{9} \eta[i] + \frac{2}{5} \sum_{i=10}^{18} \eta[i] + \frac{3}{5} \sum_{i=19}^{20} \eta[i] + \frac{4}{5} \sum_{i=21}^{23} \eta[i] \right)}. \tag{31}$$

Let $\widetilde{\xi}[i] = 9\xi[i]/\sigma^2$, $i = 1, 2, \ldots, 9$. It can be easily determined that $\widetilde{\xi}[i]$ is a central chi-squared random variable with two degrees of freedom as well. Meanwhile, the variance of $\widetilde{\xi}[i]$ is equal to 1, which is constant and independent of the noise power.

The same operation as that for the denominator in (18) is applied. Thus, the expression for the test statistic $T$ can be written as follows:

$$T = \frac{\sum_{i=1}^{9} \widetilde{\xi}[i]}{\sum_{i=1}^{23} \widetilde{\eta}[i]} \triangleq \frac{T_{num}}{T_{den}}. \tag{32}$$

According to (32), $T_{num}$ is the sum of nine independent central chi-squared variables with two degrees of freedom, resulting in the chi-squared distribution with 18 degrees of freedom. Hence, the p.d.f of $T_{num}$ under the null hypothesis $H_0$ is given by

$$f_{num}(x\,|H_0) = \frac{1}{2^9 \times 8!}x^8 e^{-\frac{x}{2}}, \quad x \geq 0. \tag{33}$$

In addition, the p.d.f of $T_{den}$ under $H_0$ denoted by $f_{den}(y\,|H_0)$ has the same expression as that under $H_1$, which is represented in (23). Thus, we can derive the p.d.f of the test statistic $T$ under $H_0$ as follows:

$$\begin{aligned} f_T(z\,|H_0) &= \int_0^{+\infty} y f_{num}(yz\,|H_0) f_{den}(y\,|H_0)\mathrm{d}y \\ &= L_2 z^8 \sum_{k=1}^{4}\sum_{l=1}^{r_k} \frac{\Psi_{k,l,r}}{(r_k-l)!}(-1)^{r_k-l}\frac{(r_k-l+9)!}{\left(\frac{z}{2}+\frac{1}{\sigma_k^2}\right)^{r_k-l+10}}, \end{aligned} \tag{34}$$

where $L_2 = L_1/(2^9 \times 8!)$ is a constant, and the integral in (34) can be calculated through integration by parts.

For a given threshold $\lambda_c$, the false alarm probability of the CFAR detection can be computed as follows:

$$P_{f1} = \int_{\lambda_c}^{+\infty} f_T(z\,|H_0)\mathrm{d}y. \tag{35}$$

Furthermore, as we can see from (34), $f_T(z\,|H_0)$ is independent of the noise power $\sigma^2$, and so is the probability of false alarm $P_{f1}$. The objective of CFAR processing is realized. According to (35), it is notable that the threshold $\lambda_c$ can be determined based on the corresponding false alarm probability.

### D. SIMULATIONS

In this section, Monte Carlo simulations are carried out to validate the theoretical expressions of false alarm probability $P_{f1}$ and success probability $P_C$.

Fig. 4(a) shows the simulation results for the false alarm probability versus the threshold and the simulation is conducted $10^5$ times. The red line in Fig. 4(a) represents the theoretical curve calculated based on (35). It is clear that the simulation results match perfectly with the theoretical one. The probability of false alarm is close to $10^{-7}$ when the threshold is set to 8. As mentioned above, the false alarm probability is just a function of the threshold, and in turn the detection threshold can be determined according to the desired probability of false alarm.

Fig. 4(b) illustrates the probabilities of success against the threshold varying from 1 to 35 for different $E_b/N_0$. Note that throughout the simulations of this paper, the energy per bit to noise power spectral density ratio, i.e. $E_b/N_0$, is utilized exclusively to represent the power difference between signal and noise. It is because that SNR and $E_b/N_0$ can be derived from each other for a fixed bandwidth. It can be observed from Fig. 4(b) that the Monte Carlo simulation results are very close to the corresponding theoretical curves, permitting to validate analytic expression for success probability of (28). The probability of success decreases dramatically as the threshold increases. When the case of $E_b/N_0 = 8$ dB is compared with $E_b/N_0 = 12$ dB, additional $\lambda_c$ of approximately 7.5 is required to reach the same success probability equal to 0.9.

Next, we fix the detection threshold $\lambda_c$, and the curves of success probability in terms of $E_b/N_0$ are depicted in Fig. 4(c), in which a great agreement between simulation results and theoretical ones is observed. The uppermost curve in Fig. 4(c) is the result for $\lambda_c = 4$ and the other two are for $\lambda_c = 6$ and $\lambda_c = 8$ respectively. In the case of $\lambda_c = 8$, we have noticed that the success probability of 0.9 is obtained at $E_b/N_0 = 10$ dB, whereas for $\lambda_c = 4$, there is a 3 dB gain to have the same detection performance.

By using (28) and (35), we can plot the theoretical curves of success probability $P_C$ versus false alarm probability $P_{f1}$ (i.e. Receiver Operating Characteristic curves, ROC) for different $E_b/N_0$ varying from 4 to 8 dB, as shown in Fig. 4(d). The corresponding simulation results are presented as well. It is notable that the CFAR detection has an excellent detection performance with low SNRs and an acceptable false alarm probability.

## IV. DETERMINISTIC SYMBOL MATCH

For every ADS-B message with DF = 17, the sequence $\mathbf{e}$ of (5) is identical. If $\mathbf{e}$ is regarded as a special PPM signal and is decoded accordingly, we can obtain a symbol pattern represented as

$$\theta = [1, 1, X_1, 0, 0, X_2, X_3, X_4, 1, 0, 0, 0, 1], \tag{36}$$

where $X_i$, $(i = 1, 2, 3, 4)$ is null symbol, as is illustrated in Fig. 5. Further, the symbol pattern $\theta$ can be divided into two parts: the deterministic pattern $\theta_{\boldsymbol{d}} = [1, 1, 0, 0, 1, 0, 0, 0, 1]$ and the null pattern $\theta_{\boldsymbol{n}} = [X_1, X_2, X_3, X_4]$. Herein, $\theta_{\boldsymbol{d}}$ consists of nine deterministic symbols and is used for deterministic symbol match and consistent power test. The null pattern $\theta_{\boldsymbol{n}}$ is utilized for null symbol validation.

Using the above CFAR detection, we can obtain the sample position corresponding to the end of the characteristic word $\mathbf{e}$, where the test statistic $T$ is larger than the threshold $\lambda_c$. Then we need to examine whether there are nine deterministic symbols at the specific positions with respect to the obtained sample position. In the signal model established in this paper, those specific positions are denoted by $\boldsymbol{\ell} = [1, 2, 3, 4, 7, 8, 9, 10, 17, 18, 19, 20, 21, 22, 23, 24, 25, 26]$, comprising 18 elements totally. Denote the deterministic pattern decoded from the received signal by $\widetilde{\theta}_{\boldsymbol{d}} = [\widetilde{\theta}_d[1], \widetilde{\theta}_d[2], \ldots, \widetilde{\theta}_d[9]]$. The $k$th $(k = 1, 2, \ldots, 9)$ symbol is declared as "1" or "0" by comparing the values of two samples in both the chips of a symbol interval, i.e., if $y[\ell[2k-1]L] \geq y[\ell[2k]L]$, we have $\widetilde{\theta}_d[k] = 1$, otherwise $\widetilde{\theta}_d[k] = 0$. When the decoded pattern $\widetilde{\theta}_{\boldsymbol{d}}$ matches with the standard

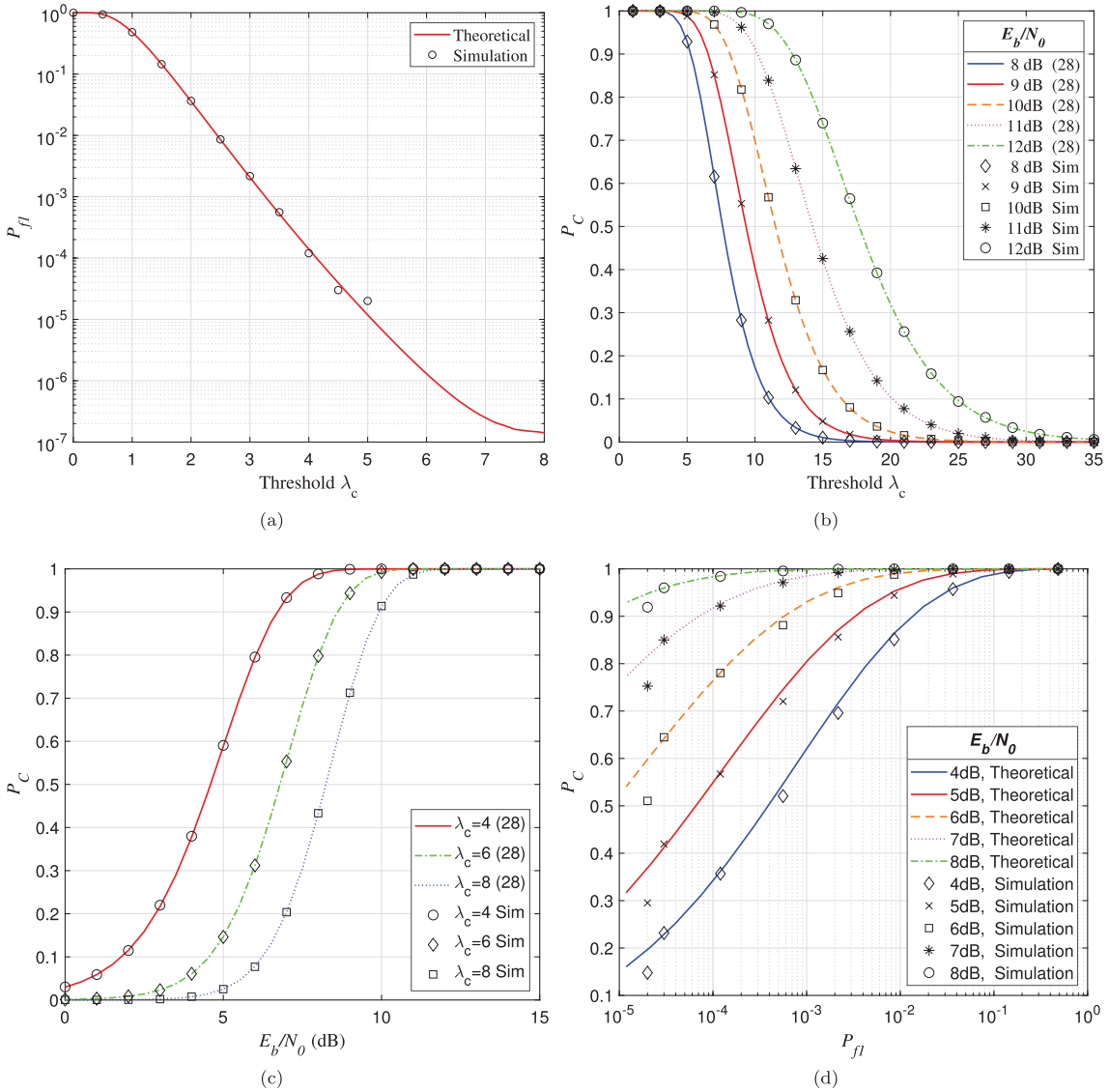


**FIGURE 4.** (a) False alarm probability $P_{f1}$ vs $\lambda_c$, (b) Success probability $P_C$ vs $\lambda_c$, (c) Success probability $P_C$ vs $E_b/N_0$, (d) ROC curve of CFAR detection.

deterministic pattern $\theta_d$, the third criterion consistent power test is activated.

Next, we derive the probability that the decoded pattern $\widetilde{\theta}_d$ matches with the standard pattern $\theta_d$, which is denoted by $P_M$. Actually, this probability is determined by the error probability for the described decoding scheme of PPM signals. Considering that PPM signals are also binary orthogonal signals, we can find the probability of a bit error for noncoherent detection of orthogonal signals in [30], i.e.,

$$P_e = \frac{1}{2}\exp\left(-\frac{9A^2}{4\sigma^2}\right). \tag{37}$$

Due to the independence of the nine deterministic symbols, we can calculate the probability $P_M$ easily as follows

$$P_M = (1-P_e)^9 = \left(1-\frac{1}{2}\exp\left(-\frac{9A^2}{4\sigma^2}\right)\right)^9, \tag{38}$$

which is a function of the SNR as well.

Finally, Monte Carlo simulation is carried out to validate the analytic expression for success probability of deterministic symbol match $P_M$. Fig. 6 shows both the theoretical curve expressed in (38) and the simulated one. It is clear that the success probability $P_M$ is above 0.9 when $E_b/N_0$ is larger than 9 dB.

## V. CONSISTENT POWER TEST

### A. DESCRIPTION

When the third criterion, consistent power test, is activated, it implies that there is a deterministic pattern at specific positions, i.e., $\widetilde{\theta}_d$ matches with $\theta_d$. For each deterministic symbol interval, we select the larger sample from the two values used to determine "1" or "0", either in the leading chip or in the trailing chip. The index vector of the nine selected samples are characterized by $\boldsymbol{\alpha}$ of (13). We can thus obtain a sample set consisting of the nine larger values,

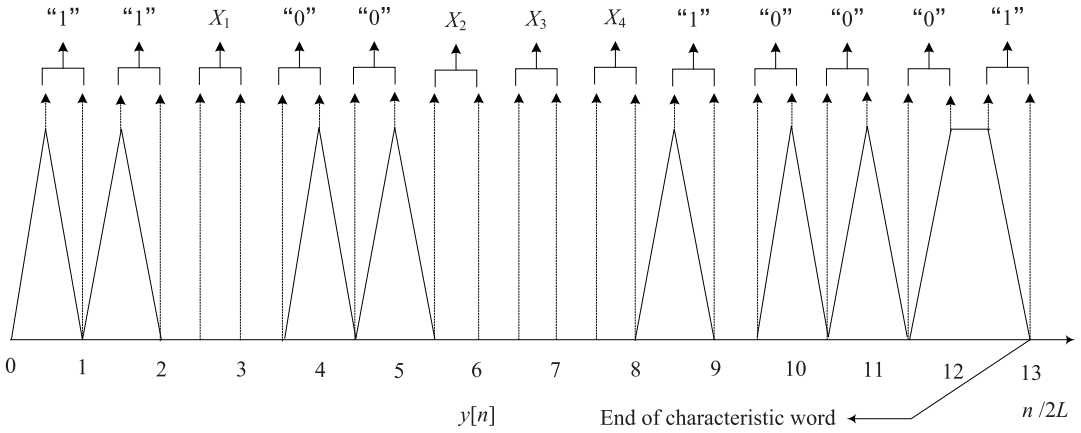


**FIGURE 5.** Sketch of deterministic symbol match.

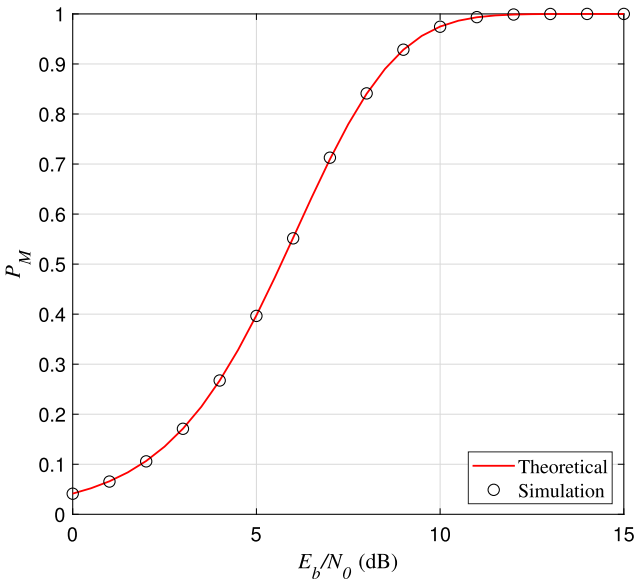


**FIGURE 6.** Success probability $P_M$ vs $E_b/N_0$.

which can be represented as

$$\boldsymbol{\vartheta} = \{y[\alpha[i]L], i = 1, 2, \ldots, 9\}. \tag{39}$$

The elements in $\boldsymbol{\vartheta}$ correspond to the nine peak values illustrated in Fig. 5.

In the sample set, let $\vartheta_{max}$ be the maximum and $\vartheta_{min}$ be the minimum of the nine peak values. By comparing the ratio of $\vartheta_{max}$ to $\vartheta_{min}$ with a predetermined threshold $\lambda_p$, the success or failure of consistent power test would be declared. To be specific, if $\vartheta_{max}/\vartheta_{min}$ is smaller than $\lambda_p$, the consistent power test is considered successful and the final criterion, null symbol validation, will take effect.

The consistent power test is beneficial to reducing the probability of false alarm significantly. For instance, when the reference sequence and the preamble of received signal are aligned partly and the decoded pattern $\widetilde{\Theta}_d$ matches with $\Theta_d$ by coincidence, some of the nine peak values are generated by noise. The minimum of the set $\vartheta_{min}$ would then be far smaller than the maximum $\vartheta_{max}$, with the result that $\vartheta_{max}/\vartheta_{min}$ is larger than $\lambda_p$. Therefore, this kind of false alarm can be suppressed effectively.

### B. ANALYSIS OF CONSISTENT POWER TEST

Under the hypothesis $H_1$, the element in the set $\boldsymbol{\vartheta}$ is indeed the case of $y[n]$ with $d[\alpha[i]] = 1$ and $n = \alpha[i]L$ for $i = 1, 2, \ldots, 9$. As analyzed in section III-B, the nine variables in $\boldsymbol{\vartheta}$ are independent and identically distributed and obey the non-central chi-squared distribution with two degrees of freedom and a non-centrality parameter equal to $A^2$. The p.d.f can be thus expressed as

$$f(x\,|H_1) = \frac{9}{2\sigma^2}\exp\left(-\frac{9(x+A^2)}{2\sigma^2}\right) I_0\left(\frac{9A}{\sigma^2}\sqrt{x}\right), \quad x \geq 0, \tag{40}$$

where $I_0(\cdot)$ is the modified Bessel function of the first kind and zero order. Its cumulative distribution function (CDF) can be given by

$$F(z\,|H_1) = \int_0^z f(x\,|H_1)\mathrm{d}x = 1 - Q_1\left(\frac{3A}{\sigma}, \frac{3\sqrt{z}}{\sigma}\right), \tag{41}$$

where $Q_1(\cdot,\cdot)$ is the first order Marcum $Q$ function.

Obviously, $\vartheta_{max}$ is the largest order statistic among the nine variables in $\boldsymbol{\vartheta}$, of which the p.d.f can be expressed as [31]

$$\begin{aligned} f_{max}(x\,|H_1) &= 9\,(F(x\,|H_1))^8 f(x\,|H_1) \\ &= 9\left(1 - Q_1\left(\frac{3A}{\sigma}, \frac{3\sqrt{x}}{\sigma}\right)\right)^8 f(x\,|H_1). \end{aligned} \tag{42}$$

Similarly, the smallest order statistic $\vartheta_{min}$ has the p.d.f represented as [31]

$$\begin{aligned} f_{min}(y\,|H_1) &= 9\,(1 - F(y\,|H_1))^8 f(y\,|H_1) \\ &= 9\left(Q_1\left(\frac{3A}{\sigma}, \frac{3\sqrt{y}}{\sigma}\right)\right)^8 f(y\,|H_1) \end{aligned} \tag{43}$$

Let $R = \vartheta_{max}/\vartheta_{min}$, $\vartheta_{max} \geq \vartheta_{min} > 0$. Note that $R \geq 1$ and the ratio distribution has the p.d.f indicated as

$$f_R(z\,|H_1) = \int_0^{+\infty} y f_{max}(yz\,|H_1) f_{min}(y\,|H_1)\mathrm{d}y. \tag{44}$$

Given a preset threshold $\lambda_p$, the success probability of consistent power test $P_T$ is given by

$$P_T = \int_1^{\lambda_p} f_R(z\,|H_1)\mathrm{d}z. \tag{45}$$

Here, the value of $P_T$ can be calculated by numerical integration.

### C. FALSE ALARM PROBABILITY $P_{f3}$

Under the null hypothesis $H_0$, the nine variables in the set $\boldsymbol{\vartheta}$ are generated by noise, and subject to central chi-squared distribution with two degrees of freedom, of which the p.d.f can be written as

$$f(x\,|H_0) = \frac{9}{2\sigma^2}\exp\left(-\frac{9x}{2\sigma^2}\right), \quad x \geq 0. \tag{46}$$

The CDF is then given by

$$F(z\,|H_0) = 1 - \exp\left(-\frac{9z}{2\sigma^2}\right). \tag{47}$$

Similarly, the largest order statistic $\vartheta_{max}$ and the smallest order statistic $\vartheta_{min}$ under $H_0$ have the p.d.f

$$\begin{aligned} f_{max}(x\,|H_0) &= \frac{81}{2\sigma^2}\exp\left(-\frac{9x}{2\sigma^2}\right)\left(1-\exp\left(-\frac{9x}{2\sigma^2}\right)\right)^8 \\ f_{min}(y\,|H_0) &= \frac{81}{2\sigma^2}\exp\left(-\frac{81y}{2\sigma^2}\right). \end{aligned} \tag{48}$$

Thus, the p.d.f of $R = \vartheta_{max}/\vartheta_{min}$ under $H_0$ is obtained by

$$f_R(z\,|H_0) = 81\int_0^{+\infty} t\,(1-\exp(-tz))^8\exp(-t(z+9))\,\mathrm{d}t. \tag{49}$$

It is notable that $f_R(z\,|H_0)$ is independent of noise power $\sigma^2$. When $R = \vartheta_{max}/\vartheta_{min}$ under the null hypothesis $H_0$ is less than or equal to the given threshold $\lambda_p$, it implies that the third criterion, consistent power test, is considered successful in the case of noise only. To some extent, this is a false alarm, and its probability which is denoted by $P_{f3}$ can be calculated by integrating the $f_R(z\,|H_0)$ from 1 to $\lambda_p$, i.e.,

$$P_{f3} = \int_1^{\lambda_p} f_R(z\,|H_0)\mathrm{d}z. \tag{50}$$

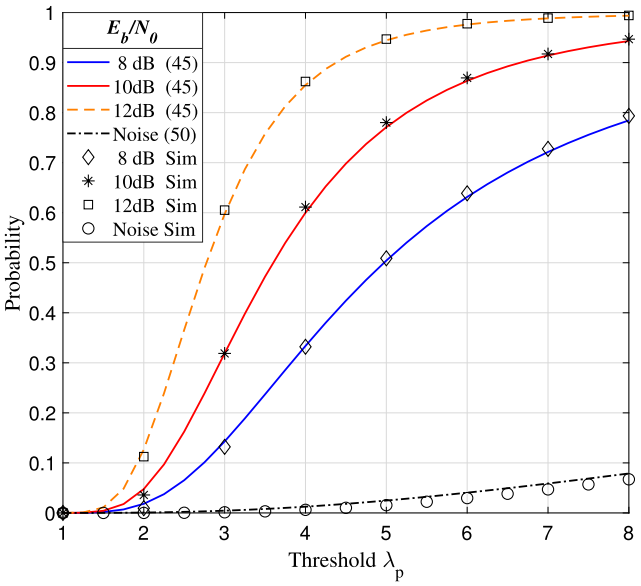


**FIGURE 7.** Success probability $P_T$ and false alarm probability $P_{f3}$.

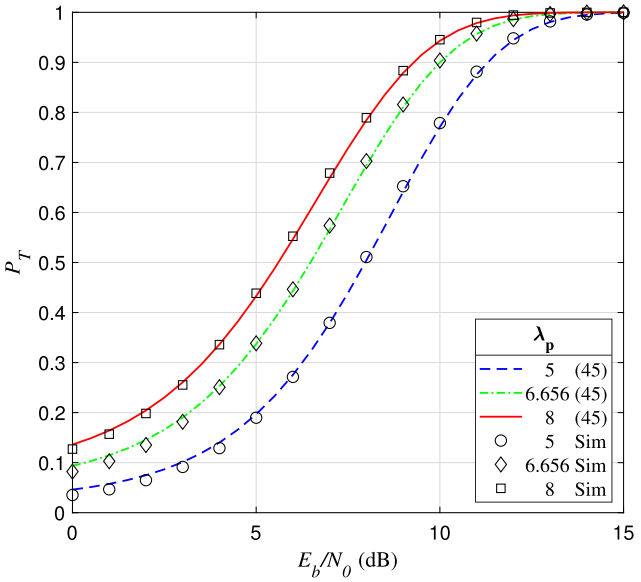


**FIGURE 8.** Success probability $P_T$ vs $E_b/N_0$.

### D. SIMULATIONS

Both the success probability $P_T$ and false alarm probability $P_{f3}$ are validated by Monte Carlo simulations in Fig. 7. In this simulation, $E_b/N_0$ are set to 8, 10, and 12 dB respectively. When $E_b/N_0 = 10$ dB and $P_T = 0.9$, the corresponding threshold can be calculated by solving the equation (45), that is $\lambda_p = 6.656$. The downmost curve in Fig. 7 corresponds to the null hypothesis $H_0$.

Fig. 8 illustrates the probability of success $P_T$ against $E_b/N_0$ for different threshold $\lambda_p$, including the theoretical curves and simulated ones. It is notable that the performance will be improved with the growth of threshold.

## VI. NULL SYMBOL VALIDATION

### A. DESCRIPTION

The final criterion, null symbol validation, is activated if all the previous criteria are successful. It is specially designed for the null pattern $\theta_n$ mentioned in section IV. Generally, there are no triangular pulses in the four null symbol intervals. Null symbol validation is thus to confirm that there is no energy at those positions.

A dynamic threshold $\tau$ is exploited and defined as the average of nine peak values in the sample set $\vartheta$, i.e.,

$$\tau = \frac{1}{9}\sum_{i=1}^{9} y[\alpha[i]L]. \tag{51}$$

As shown in Fig. 5, each null symbol $X_k$ $(k = 1, 2, 3, 4)$ in the null pattern $\theta_n$ comprises two samples located in the leading chip and in the trailing chip respectively. There are totally 8 samples for the four null symbols, of which the index vector is characterized by $\beta = [5, 6, 11, 12, 13, 14, 15, 16]$. For the $k$th $(k = 1, 2, 3, 4)$ null symbol $X_k$, if both the samples in the corresponding symbol interval are no more than half of the dynamic threshold $\tau$, i.e., $y[\beta[2k-1]L] \le \tau/2$ and $y[\beta[2k]L] \le \tau/2$, $X_k$ will be identified as empty. Otherwise, it is nonempty. If the total number of empty symbols in $\theta_n$ is greater than or equal to 2, null symbol validation is considered successful and it is announced that an ADS-B preamble has been detected.

Null symbol validation is requisite for the preamble detection. The false alarm would occur probably when there is a pattern identical to the deterministic one $\theta_d$ in the data block of an ADS-B message by accident. However, there are data pulses in the four symbol intervals under the circumstances, leading to the failure of null symbol validation. Hence, this kind of false alarm generated by the data block shall be suppressed to some extent.

### B. ANALYSIS OF NULL SYMBOL VALIDATION

First of all, the distribution of dynamic threshold $\tau$ is investigated. Under the hypothesis $H_1$, each variable $y[\alpha[i]L]$ $(i = 1, 2, \ldots, 9)$ in the sample set $\vartheta$ obeys the non-central chi-squared distribution with two degrees of freedom and a non-centrality parameter equal to $A^2$. The mean and variance of $y[\alpha[i]L]$ can be obtained by [32]

$$\begin{cases} \mu_Y = \frac{2}{9}\sigma^2 + A^2 \\ \sigma_Y^2 = \frac{4}{81}\sigma^4 + \frac{4}{9}\sigma^2 A^2. \end{cases} \tag{52}$$

In addition, each $y[\alpha[i]L]$ is independent and identically distributed, and we can make the approximation that the average of the sample set $\tau$ obeys the normal distribution approximately according to the central-limit theorem, namely $\tau \sim N(\mu_Y,\ \sigma_Y^2/9)$. The p.d.f is thus given by

$$f_\tau(t) = \frac{1}{\sqrt{2\pi\sigma_Y^2/9}} \exp\left(-\frac{9}{2\sigma_Y^2}(t-\mu_Y)^2\right), \quad t \ge 0. \tag{53}$$

On the other hand, there are totally 8 samples for the four null symbols, and each of them is a central chi-squared random variable with two degrees of freedom and a p.d.f indicated as

$$f_X(x) = \frac{9}{2\sigma^2}\exp\left(-\frac{9x}{2\sigma^2}\right), \quad x \ge 0. \tag{54}$$

Given the threshold $\tau$, for the single sample, the probability that it dose not exceed the threshold can be calculated as

$$P_0 = \int_0^{\tau/2} f_X(x)\mathrm{d}x = 1 - \exp\left(-\frac{9\tau}{4\sigma^2}\right). \tag{55}$$

Note that a null symbol $X_k$ $(k = 1, 2, 3, 4)$ consists of two independent samples, the probability that $X_k$ is declared empty can be denoted by

$$P_{ept} = P_0^2 = \left(1 - \exp\left(-\frac{9\tau}{4\sigma^2}\right)\right)^2. \tag{56}$$

Equivalently, the probability that it is declared nonempty can be given by

$$P_{nept} = 1 - P_{ept} = 1 - \left(1 - \exp\left(-\frac{9\tau}{4\sigma^2}\right)\right)^2 \tag{57}$$

Further, for the fixed threshold $\tau$, the probability that the null symbol validation is considered successful can be expressed as

$$\begin{aligned} P_\tau &= P_{ept}^4 + C_4^1 P_{nept} P_{ept}^3 + C_4^2 P_{nept}^2 P_{ept}^2 \\ &= \sum_{k=0}^{2} C_4^k P_{nept}^k P_{ept}^{4-k}. \end{aligned} \tag{58}$$

Here, the notation $C_4^k$ has the same definition as that in (24).

Considering that the dynamic threshold $\tau$ is actually a random variable, we need to calculate the mathematical expectation of $P_\tau$ in order to obtain the success probability $P_N$, that is,

$$\begin{aligned} P_N &= E\{P_\tau\} \\ &= \int_0^{+\infty} P_\tau f_\tau(\tau)\mathrm{d}\tau \\ &= \int_0^{+\infty} \sum_{k=0}^{2} C_4^k P_{nept}^k P_{ept}^{4-k} f_\tau(\tau)\mathrm{d}\tau, \end{aligned} \tag{59}$$

where $E\{\cdot\}$ is the expectation operator.

The analytic expression for $P_N$ of (59) is validated by Monte Carlo simulations in Fig. 9, from which the consistency between the theoretical and simulation results is observed. It is notable that $P_N$ approaches 1 when $E_b/N_0$ is over 7 dB, which implies that the null symbol validation is successful automatically.

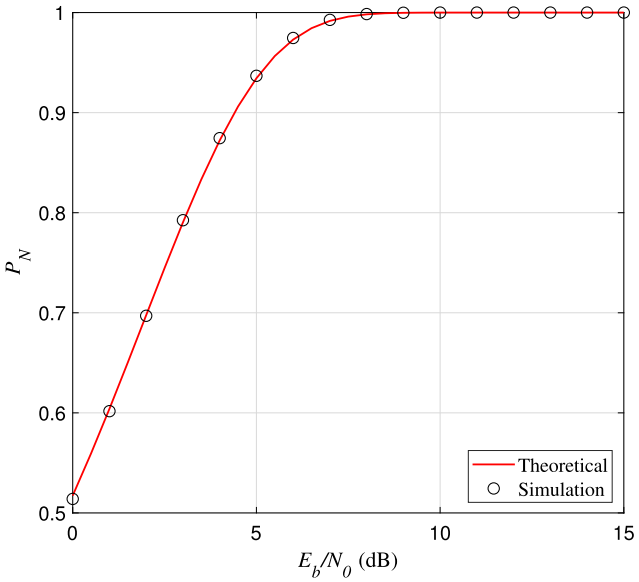


**FIGURE 9.** Success probability $P_N$ vs $E_b/N_0$.

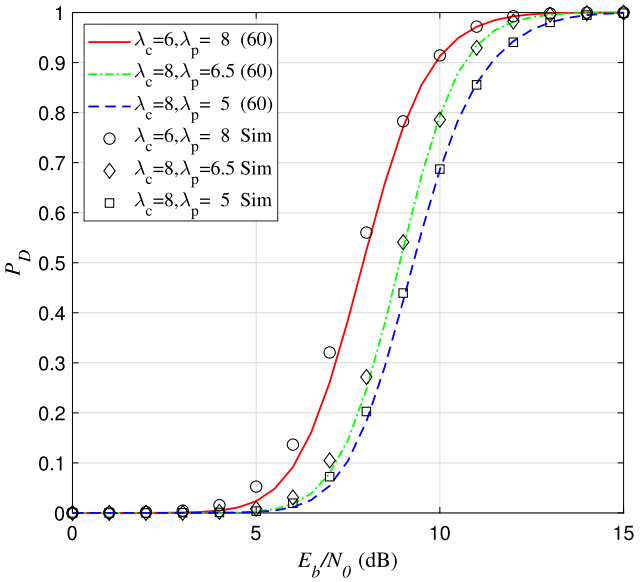


**FIGURE 11.** Detection probability $P_D$ vs $E_b/N_0$.

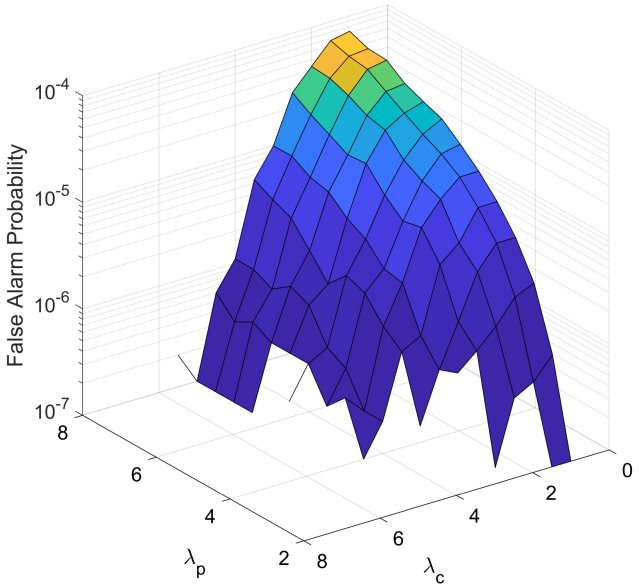


**FIGURE 10.** False alarm probability vs $\lambda_c$ and $\lambda_p$.

## VII. SIMULATIONS AND RESULTS

### A. FALSE ALARM PROBABILITY

First of all, the false alarm probability of the proposed multi-criteria preamble detection algorithm is investigated by Monte Carlo simulations. Fig. 10 shows the simulation results for the probability of false alarm in terms of thresholds. The threshold $\lambda_c$ varies from 1 to 8, and $\lambda_p$ varies from 2 to 8. For each pair of $\lambda_c$ and $\lambda_p$, the simulation is conducted $10^7$ times. It can be observed from Fig. 10 that as the threshold $\lambda_c$ increases and $\lambda_p$ decreases, the false alarm probability of the proposed algorithm will decrease. The largest simulated false alarm probability is approximately $7 \times 10^{-5}$ when $\lambda_c$ is equal to 1 and $\lambda_p$ is equal to 8. In addition, it is clear that the false alarm probability is smaller than $10^{-7}$ if $\lambda_c$ is larger than 4.5.

### B. VALIDATION OF DETECTION PROBABILITY

In the previous sections, we have already developed the success probability for each criterion, i.e., $P_C$, $P_M$, $P_T$, and $P_N$. The detection probability of the proposed multi-criteria preamble detection algorithm is thus expressed as

$$P_D = P_C \cdot P_M \cdot P_T \cdot P_N. \tag{60}$$

Herein, $P_D$ depends on three parameters: $\lambda_c$, $\lambda_p$, and $E_b/N_0$.

Fig. 11 shows the detection probability versus $E_b/N_0$ for different pairs of $\lambda_c$ and $\lambda_p$, including the theoretical curves and simulated ones. For each $E_b/N_0$ with fixed $\lambda_c$ and $\lambda_p$, the proposed detection algorithm is simulated $10^4$ times. It is expected from Fig. 11 that the simulation results are very close to the theoretical curves, permitting to validate the analytic expression of detection probability $P_D$ in (60). The top curve in Fig. 11 is the case of $\lambda_c = 6$ and $\lambda_p = 8$, and the bottom is $\lambda_c = 8$ and $\lambda_p = 5$. The middle curve is $\lambda_c = 8$ and $\lambda_p = 6.5$. By comparing the detection performance of the three cases, we have noticed that for a certain $E_b/N_0$, the probability of detection $P_D$ will increase with the decrease of $\lambda_c$ and the growth of $\lambda_p$.

### C. PERFORMANCE COMPARISON

As mentioned in [23], the re-triggering function of the enhanced squitter reception technique is of great importance in that it will reject certain preamble detections when a subsequent stronger signal is received. It is also included in the proposed multi-criteria preamble detection algorithm in this paper. When all the four criteria above are satisfied, an ADS-B preamble is declared to be detected, and a reference power level is generated by averaging the squared amplitudes of the nine deterministic symbols, i.e., the dynamic threshold $\tau$ in section VI-A. After an ADS-B preamble is identified, the preamble detection process continues to be

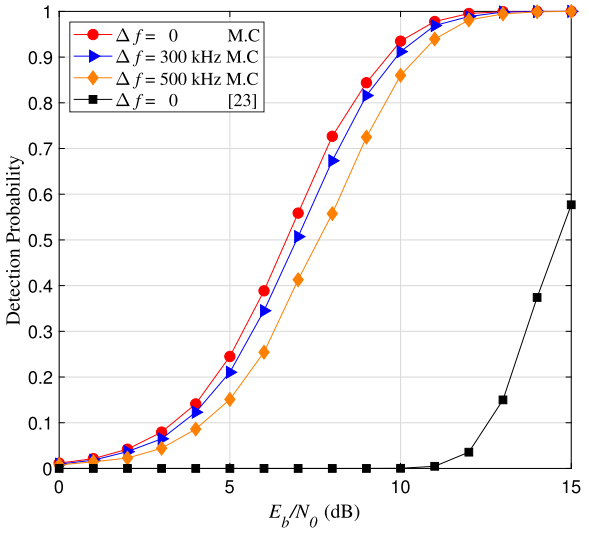


**FIGURE 12.** Comparison of detection probability.

applied to search for later preambles, and all of the proposed criteria are examined. If a particular preamble detection has survived these tests, we compare its reference power level against any earlier signal currently being processed. If the new signal is stronger by 3 dB or more, the earlier preamble is then discarded and the new signal can proceed. Otherwise, the new signal is discarded.

Next, the comparison between the detection performance of the proposed algorithm and the enhanced squitter reception technique recommended in [23] is investigated. For each $E_b/N_0$, there are $10^4$ ADS-B messages transmitted. The re-triggering function is applied for both the detection algorithms. By counting the number of correctly detected ADS-B messages, we can obtain the corresponding probability of detection. For the enhanced algorithm in [23], the optimal detection performance can be obtained via adjusting the detection threshold and is depicted in Fig. 12 as the downmost curve. The uppermost curve represents the detection probability of the proposed multi-criteria preamble detection algorithm (referred to as M.C). Both are with no frequency offset. It is notable that the detection probability of the algorithm in [23] is deteriorated dramatically at low SNRs. Although the enhanced squitter reception technique has an excellent performance with sufficient SNRs, the detection probability is approximately 0.6 at $E_b/N_0 = 15$ dB. However, for the proposed algorithm, the detection probability is over 0.9 when $E_b/N_0$ is equal to 10 dB, which is more suitable for satellite-based ADS-B application.

Fig. 12 also illustrates the influence of frequency offset $\Delta f$ on the detection probability of the proposed algorithm. The frequency offset is set to 0, 300 kHz, and 500 kHz respectively. It can be seen from Fig. 12 that the detection probability for $\Delta f = 0$ is quite close to that for $\Delta f = 300$ kHz. In addition, when comparing the case of $\Delta f = 500$ kHz with $\Delta f = 0$, the deterioration of detection probability by 1 dB is observed as well.

## VIII. CONCLUSION

In order to solve the problem of low SNR in satellite-based ADS-B application, we have proposed a novel multi-criteria preamble detection algorithm for ADS-B signals with DF set to 17. The CFAR property of the proposed algorithm makes it robust against the noise fluctuation, improving the stability and reliability of the detection algorithm. The combination of four criteria is beneficial to reducing the false alarm effectively. Moreover, the detailed analysis in this paper provides theoretical formulae for the determination of the thresholds $\lambda_c$ and $\lambda_p$, and the analytic expression of detection probability $P_D$ is derived. Simulation results show that the proposed algorithm has an excellent detection performance at low SNRs, and is suitable for the satellite-based application.

## REFERENCES

[1] J. Tang, "Analysis and improvement of traffic alert and collision avoidance system," *IEEE Access*, vol. 5, pp. 21419–21429, 2017.
[2] B. Paul, A. R. Chiriyath, and D. W. Bliss, "Survey of RF communications and sensing convergence research," *IEEE Access*, vol. 5, pp. 252–270, 2017.
[3] W. R. Richards, K. O'Brien, and D. C. Miller, "New air traffic surveillance technology," *Boeing Aero Quart.*, vol. 2, pp. 6–13, 2nd Quart., 2010.
[4] A. A. Barsheshat, "Implementation of ADS-B systems—Benefits and considerations," in *Proc. Tyrrhenian Int. Workshop Digit. Commun.-Enhanced Surveill. Aircr. Vehicles*, 2011, pp. 197–201.
[5] A. Smith, R. Cassell, T. Breen, R. Hulstrom, and C. Evers, "Methods to provide system-wide ADS-B back-up, validation and security," in *Proc. IEEE/AIAA 25th Digit. Avionics Syst. Conf.*, Oct. 2006, pp. 1–7.
[6] E. Hableel, J. Baek, Y.-J. Byon, and D. S. Wong, "How to protect ADS-B: Confidentiality framework for future air traffic communication," in *Proc. IEEE Conf. Comput. Commun. Workshops (INFOCOM WKSHPS)*, 2015, pp. 155–160.
[7] D. McCallie, J. Butts, and R. Mills, "Security analysis of the ADS-B implementation in the next generation air transportation system," *Int. J. Crit. Infrastruct. Protect.*, vol. 4, no. 2, pp. 78–87, Aug. 2011.
[8] M. Mosca and S. Hoffenson, "Using agent-based modeling to understand stakeholder interactions in the rollout of nextgen by the federal aviation administration," in *Proc. Annu. IEEE Int. Syst. Conf. (SysCon)*, Apr. 2017, pp. 1–8.
[9] M. Schäfer, M. Strohmeier, V. Lenders, I. Martinovic, and M. Wilhelm, "Bringing up OpenSky: A large-scale ADS-B sensor network for research," in *Proc. 13th Int. Symp. Inf. Process. Sensor Netw.*, 2014, pp. 83–94.
[10] C. Rekkas and M. Rees, "Towards ADS-B implementation in Europe," in *Proc. Tyrrhenian Int. Workshop Digit. Commun.-Enhanced Surveill. Aircr. Vehicles*, 2008, pp. 1–4.
[11] M. Strohmeier, M. Schafer, V. Lenders, and I. Martinovic, "Realities and challenges of NextGen air traffic management: The case of ADS-B," *IEEE Commun. Mag.*, vol. 52, no. 5, pp. 111–118, May 2014.
[12] K. Werner, J. Bredemeyer, and T. Delovski, "ADS-B over satellite: Global air traffic surveillance from space," in *Proc. Tyrrhenian Int. Workshop Digit. Commun.-Enhanced Surveill. Aircr. Vehicles (TIWDC/ESAV)*, Sep. 2014, pp. 47–52.
[13] B. G. Knudsen, M. Jensen, A. Birklykke, P. Koch, J. Christiansen, K. Laursen, L. Alminde, and Y. Le Moullec, "ADS-B in space: Decoder implementation and first results from the GATOSS mission," in *Proc. 14th Biennial Baltic Electron. Conf. (BEC)*, 2014, pp. 57–60.
[14] P. Noschese, S. Porfili, and S. Di Girolamo, "ADS-B via Iridium next satellites," in *Proc. Tyrrhenian Int. Workshop Digit. Commun.-Enhanced Surveill. Aircr. Vehicles*, Sep. 2011, pp. 213–218.
[15] M. Strohmeier, V. Lenders, and I. Martinovic, "On the security of the automatic dependent surveillance-broadcast protocol," *IEEE Commun. Surveys Tuts.*, vol. 17, no. 2, pp. 1066–1087, 2nd Quart., 2015.
[16] M. Sopata and P. Kejik, "Enhanced techniques for improved ADS-B messages reception," in *Proc. IEEE/AIAA 34th Digit. Avionics Syst. Conf. (DASC)*, Sep. 2015, pp. 2E1-1–2E1-8.

[17] N. Petrochilos, G. Galati, and E. Piracci, "Separation of SSR signals by array processing in multilateration systems," *IEEE Trans. Aerosp. Electron. Syst.*, vol. 45, no. 3, pp. 965–982, Jul. 2009.
[18] M. Zhou and A.-J. van der Veen, "Improved blind separation algorithm for overlapping secondary surveillance radar replies," in *Proc. 4th IEEE Int. Workshop Comput. Adv. Multi-Sensor Adapt. Process. (CAMSAP)*, Dec. 2011, pp. 181–184.
[19] N. Petrochilos and A.-J. van der Veen, "Algebraic algorithms to separate overlapping secondary surveillance radar replies," *IEEE Trans. Signal Process.*, vol. 55, no. 7, pp. 3746–3759, Jul. 2007.
[20] G. Galati, N. Petrochilos, and E. G. Piracci, "Degarbling Mode S replies received in single channel stations with a digital incremental improvement," *IET Radar, Sonar Navigat.*, vol. 9, no. 6, pp. 681–691, 2015.
[21] E. G. Piracci, N. Petrochilos, and G. Galati, "Mixed SSR sources separation exploiting sparsity: A geometrical approach," in *Proc. Eur. Radar Conf. (EuRAD)*, Sep. 2009, pp. 85–88.
[22] N. Petrochilos, E. G. Piracci, and G. Galati, "Improved MDA, a case for degarbling SSR Mode S replies," in *Proc. Tyrrhenian Int. Workshop Digit. Commun.-Enhanced Surveill. Aircr. Vehicles (TIWDC/ESAV)*, Sep. 2014, pp. 87–91.
[23] *DO-260B MOPS for 1090 MHz ES ADS-B and TIS-B*, RTCA, Washington, DC, USA, 2011.
[24] Y. Kim, J.-Y. Jo, and S. Lee, "ADS-B vulnerabilities and a security solution with a timestamp," *IEEE Aerosp. Electron. Syst. Mag.*, vol. 32, no. 11, pp. 52–61, Nov. 2017.
[25] *Annex 10 to the Convention on International Civil Aviation–Aeronautical Telecommunications. Volume IV–Surveillance Radar and Collision Avoidance Systems*, ICAO, Montreal, QC, Canada, 2014.
[26] M. K. Simon, *Probability Distributions Involving Gaussian Random Variables: A Handbook for Engineers and Scientists*. Berlin, Germany: Springer, 2007.
[27] K. Benachenhou, M. Hamadouche, and A. Taleb-Ahmed, "New formulation of GNSS acquisition with CFAR detection," *Int. J. Satell. Commun. Netw.*, vol. 35, no. 3, pp. 215–230, 2017.
[28] E. Bjornson, D. Hammarwall, and B. Ottersten, "Exploiting quantized channel norm feedback through conditional statistics in arbitrarily correlated MIMO systems," *IEEE Trans. Signal Process.*, vol. 57, no. 10, pp. 4027–4041, Oct. 2009.
[29] J. H. Curtiss, "On the distribution of the quotient of two chance variables," *Ann. Math. Statist.*, vol. 12, no. 4, pp. 409–421, 1941.
[30] J. Proakis, *Digital Communications*, vol. 4. New York, NY, USA: McGraw-Hill, 2001.
[31] H. A. David and H. N. Nagaraja, "Order statistics," in *Encyclopedia of Statistical Sciences*, vol. 9. Hoboken, NJ, USA: Wiley, 2004.
[32] E. W. Weisstein, "Noncentral chi-squared distribution," in *Sigma*, vol. 5. Kiev, Ukraine: Department of Applied Research, Institute of Mathematics of National Academy of Science of Ukraine, 2002, p. 6.

**PENG REN** received the B.S. degree in communication engineering from the Nanjing University of Science and Technology, Nanjing, China, in 2014, where he is currently pursuing the Ph.D. degree with the School of Electronic and Optical Engineering. His research interests include digital communications, signal processing, and automatic dependent surveillance broadcast.

**JIANXIN WANG** received the M.S. and Ph.D. degrees in electronic and information engineering from the Nanjing University of Science and Technology, Nanjing, China, in 1987 and 1999, respectively. Since 1987, he has been with the School of Electronic and Optical Engineering, Nanjing University of Science and Technology, a Teaching Assistant, a Lecturer, an Associate Professor, and as a Professor, since 2001. He was a Visiting Researcher with the Institute of Telecommunications, University of Stuttgart, Germany, from 2000 to 2012. His research interests include communications signal processing and software defined radio.

**HAIWEI SONG** received the B.S. degree in electronic information science and technology from the Xuzhou University of Technology, in 2009, and the Ph.D. degree in communication and information system from the Shanghai Institute of Microsystems and Information Technology (SIMIT), Chinese Academy of Sciences (CAS), in June 2014. He is currently a Senior Engineer with the Nanjing Electronic Equipment Institute.

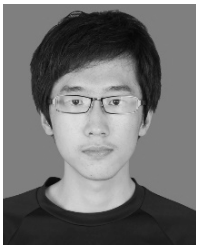

**PEIXIN ZHANG** received the B.S. degree in communications engineering from the School of Electronic and Optical Engineering, Nanjing University of Science and Technology, Nanjing, China, in 2013, where he is currently pursuing the Ph.D. degree with the School of Electronic and Optical Engineering. His main research interests include modulation recognition and automatic identification systems.

**TIAN BAN** received the M.S. degree in signal and information processing from Southeast University, Nanjing, China, in 2009, and the Ph.D. degree in communications and electronics from Telecom ParisTech, Paris, France, in 2012. From 2009 to 2012, he was with the Laboratoire de Traitement et Communication de l'Information (LTCI), the joint research laboratory between Telecom ParisTech and the Centre National de la Recherche Scientifique (CNRS), UMR. Since November 2012, he has been with the School of Electronic and Optical Engineering, Nanjing University of Science and Technology, China, where he is currently an Associate Professor. His current research interests include fault tolerant techniques in digital designs and FPGA-based digital signal processing.